

Hydrogen release of catalyzed lithium aluminum hydride by a mechanochemical reaction

Yoshitsugu Kojima<sup>a\*</sup>, Yasuaki Kawai<sup>b</sup>, Mitsuru Matsumoto<sup>b</sup>, Tetsuya Haga<sup>b</sup>

<sup>a</sup>*Institute for Advanced Materials Research, Hiroshima University, 1-3-1 Kagamiyama,*

*Higashi-Hiroshima 739-8530, Japan*

<sup>b</sup>*Toyota Central R&D Labs., Inc., Nagakute-cho, Aichi-gun, Aichi, 480-1192 Japan*

CORRESPONDING AUTHOR FOOTNOTE Tel: +81-82-424-3904, Fax: +81-82-424-5744, E-mail: [kojimay@hiroshima-u.ac.jp](mailto:kojimay@hiroshima-u.ac.jp)

Keywords: Hydrogen absorbing materials; Metal hydrides; Mechanochemical processing; Catalysis; X-ray diffraction

## **Abstract**

The effects of various catalysts on the H<sub>2</sub> release characteristics of LiAlH<sub>4</sub> were studied. It was established that the catalytic activity defined by the H<sub>2</sub> desorption capacity by a mechanochemical reaction decreased in the series TiCl<sub>3</sub>>ZrCl<sub>4</sub>>VCl<sub>3</sub>>NiCl<sub>2</sub>>ZnCl<sub>2</sub>. Transition metal trialuminides Al<sub>3</sub>X (X=Ti, Zr, V, Ni) were prepared by the mechanochemical reaction of LiAlH<sub>4</sub> and the metal chlorides, while the reaction of LiAlH<sub>4</sub> and ZnCl<sub>2</sub> yields Zn. The high catalytic activity was attributed to the lower percentage d-character and the electronegativity of those transition metals. The catalytic activity of Ni was also improved with decreasing the Ni particle size. Those catalysts were classified to two groups (1. TiCl<sub>3</sub>, ZrCl<sub>4</sub>, 2. VCl<sub>3</sub>, NiCl<sub>2</sub>, Ni, nano-Ni) from the viewpoint of the H<sub>2</sub> desorption mechanism.

## **1. Introduction**

A high-pressure MH tank with a heat-exchanger module containing  $\text{Ti}_{1.1}\text{CrMn}$  (300kg) has been developed [1-3]. The measured  $\text{H}_2$  capacity at 35 MPa was  $7.3\text{kgH}_2/180\text{L}$  (outer volume), which was 2.5 times of the high pressure tank (35MPa). This indicated that FCV with the high-pressure MH tank has a driving range of about 700 km. But, the high-pressure MH tank was heavy (420kg) because the gravimetric  $\text{H}_2$  density of  $\text{Ti}_{1.1}\text{CrMn}$  had a low value of 1.8 wt%. Storage of high  $\text{H}_2$  densities in light weight solids is a solution to this problem.

Light weight complex hydrides, such as sodium aluminum hydride ( $\text{NaAlH}_4$ ) [4-8] and lithium aluminum hydride ( $\text{LiAlH}_4$ ) [9-12] are considered attractive as hydrogen storage materials due to their large hydrogen content. The reversible hydrogen storage has been formed by doping  $\text{NaAlH}_4$  with transition metal-based catalysts [4-8]. Unfortunately, only 3-4.5 wt %  $\text{H}_2$  can be stored and recovered in reasonable time at 373-398 K [7]. For useable  $\text{H}_2$  storage,  $\text{H}_2$  absorption and desorption around room temperature is necessary. It has been reported that  $\text{LiAlH}_4$  can be easily transformed into lithium hexahydridoaluminate  $\text{Li}_3\text{AlH}_6$ , Al and  $\text{H}_2$  in the presence of catalysts or prolonged ball-milling at room temperature, which corresponds to the  $\text{H}_2$  desorption capacity of 5.3 wt% [9-12].

In this paper, the effect of various metal chlorides and elemental nickel on dehydrogenation properties of  $\text{LiAlH}_4$  will be presented.

## **2. Experimental**

### **2.1 Materials**

Lithium aluminum hydride  $\text{LiAlH}_4$  (Wako Pure Chemical Industries, Ltd. Japan, molecular weight: 37.95, density:  $0.92\text{ g/cm}^3$ ), titanium trichloride  $\text{TiCl}_3$  (Sigma-Aldrich, molecular weight:154.26), zirconium tetrachloride  $\text{ZrCl}_4$  (Wako Pure Chemical Industries,

Ltd. Japan, molecular weight: 233.03), vanadium trichloride  $\text{VCl}_3$  (Wako Pure Chemical Industries, Ltd. Japan, molecular weight: 157.30), nickel dichloride  $\text{NiCl}_2$  (Kojundo Chemical Laboratory Co., Ltd., molecular weight: 129.62), zinc chloride  $\text{ZnCl}_2$  (Wako Pure Chemical Industries, Ltd. Japan, molecular weight: 136.30), nickel Ni (Soekawa Chemicals Co., Ltd., diameter: 0.8  $\mu\text{m}$ ) and nano-Ni (Shinku Yakin Kogyo KK, Japan, diameter: approximately 20 nm) were used in this study. The mill container (Cr-Mo steel pot, internal volume: 300 mL) was loaded with 5 g of  $\text{LiAlH}_4$  and a catalyst with 95:5 or 1:1 weight ratio and 40 pieces of steel ball with a diameter of 9.5 mm. The mixtures were milled at 400 rpm for 5 min-24 h in an Ar gas pressure of 0.1 MPa at room temperature (296 K) using a planetary ball mill (Fritsch P-5).

## 2.2 Characterization

With a specially designed apparatus, temperature programmed desorption (TPD) scans were carried out at a heating rate of 2 K/min in an Ar flow of 85 mL/min.  $\text{H}_2$  desorption capacities were estimated from the peak area of the TPD spectra. Transmission electron micrographs were obtained with a high-resolution transmission electron microscope (JEOL JEM-2010FEF) using an acceleration voltage of 200 kV. The composition of specimens was measured by an energy dispersive X-ray spectroscopy (EDS). X-ray diffraction intensity curves in an inert atmosphere (Ar) were recorded with  $\text{CuK}\alpha$  radiation (50 kV, 300 mA) filtered by a monochromator using Rigaku Rint-TTR.

## 3. Results and discussion

$\text{LiAlH}_4$  doped with 5 wt% of  $\text{TiCl}_3$  desorbed only 0.3 wt% of  $\text{H}_2$  by the TPD measurement  $T < 600\text{K}$ , which indicated 7.2 wt% of  $\text{H}_2$  was desorbed during ball-milling for 24 h at room temperature. The  $\text{H}_2$  desorption capacity of ball-milled  $\text{LiAlH}_4$  doped with various metal chlorides (5 wt%, milling: 24 h) decreased in the series [ $\text{TiCl}_3$  (7.2 wt%) >

ZrCl<sub>4</sub> (6.4 wt%)>VCl<sub>3</sub> (4.8 wt%)>NiCl<sub>2</sub> (1.1 wt%)>ZnCl<sub>2</sub> (0)]. The ball-milled LiAlH<sub>4</sub> doped with ZnCl<sub>2</sub> did not destabilize LiAlH<sub>4</sub>.

The X-ray diffraction (XRD) patterns of the LiAlH<sub>4</sub> doped with metal chlorides were measured after ball milling. The XRD patterns of the ball-milled LiAlH<sub>4</sub> doped with TiCl<sub>3</sub> for 5 min, 1 h, and 24 h, the ball-milled LiAlH<sub>4</sub> for 24 h and LiAlH<sub>4</sub> together with the data of Li<sub>3</sub>AlH<sub>6</sub> [13], LiCl [13], LiH [13] and Al [13] are shown in Figure 1. The ball-milled LiAlH<sub>4</sub> for 5 min also includes Li<sub>3</sub>AlH<sub>6</sub>. Prolonged ball-milling for 1 h leads to an increase of Al content and the absence of LiAlH<sub>4</sub>. The ball-milled LiAlH<sub>4</sub> doped with TiCl<sub>3</sub> for 24 h is found to include LiCl and Al. As LiH and Al peaks overlap on the XRD curves, LiH could also be included in those specimens. The H<sub>2</sub> released from the ball-milled specimen doped with TiCl<sub>3</sub> is 7.2 wt% (7.6 g of H<sub>2</sub> per 100 g of LiAlH<sub>4</sub>). It has been reported that LiAlH<sub>4</sub> releases H<sub>2</sub> in two decomposition steps upon heating below 600 K [14].

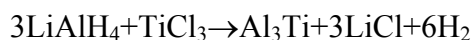


The first and the second steps can ideally release 5.3 wt% and 2.6 wt% H<sub>2</sub> relative to LiAlH<sub>4</sub>, respectively. Therefore, the XRD results indicate that the H<sub>2</sub> desorption of the LiAlH<sub>4</sub> doped with TiCl<sub>3</sub> occurs by the two-step reactions (1) and (2).

Figure 2 shows a HRTEM image of the LiAlH<sub>4</sub> doped with TiCl<sub>3</sub> ball-milled for 24 h. The ball-milled specimen that appears in the HRTEM image exhibits many dark portions. The size of the dark portions is several 10 nm. EDS analysis is specific to the region marked by square. The EDS results show that the dark portions of the transmission

electron micrograph are attributed to Ti and Al as shown in Figure 2. Since Cl is not observed in the dark portions, it is revealed that the ball-milled LiAlH<sub>4</sub> doped with TiCl<sub>3</sub> forms a nano-composite material of LiAlH<sub>4</sub> and Al-Ti, while Cl and Al were detected in the light colored portions.

Figure 3 shows XRD patterns for the ball-milled LiAlH<sub>4</sub> doped with TiCl<sub>3</sub> (taken in 1:1 weight ratio, 4:1 molar ratio) and the annealed ball-milled LiAlH<sub>4</sub> doped with TiCl<sub>3</sub> (taken in 95:5 weight ratio) together with the data of Al<sub>3</sub>Ti [13] and LiCl [13]. According to the literature [15], Al<sub>3</sub>Ti intermetallic phase crystallizes in two polymorphic modifications: tetragonal or cubic. We notice that the diffraction peaks of the ball-milled LiAlH<sub>4</sub> doped with TiCl<sub>3</sub> (50 wt%) at 2θ of 39.1°, 45.1°, 65.6° and 79.2° come from (111), (200), (220) and (311) planes of Al<sub>3</sub>Ti, in which the unit cell is cubic [11, 15]. We observe a shoulder around 2θ of 39° in the XRD pattern of the annealed specimen (423 K, 6 h). The XRD pattern of the ball-milled LiAlH<sub>4</sub> doped with TiCl<sub>3</sub> (50wt%) also shows diffraction peaks at 2θ of 30.1°, 34.9°, 50.2°, 59.6°, 62.5°, 81.5°, 84.1°, corresponding to (111), (200), (220), (311), (222), (331) and (420) planes of LiCl. Thus the reaction of LiAlH<sub>4</sub> and TiCl<sub>3</sub> can be expressed by reaction (3)

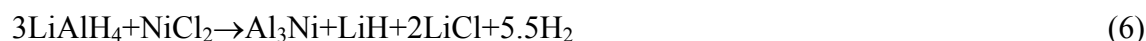
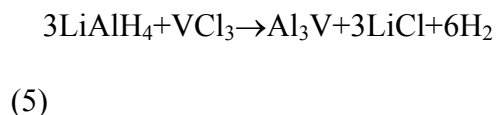
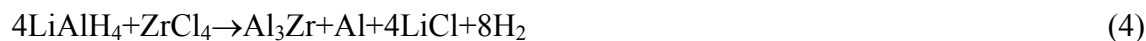


(3)

Figure 4 shows XRD patterns for ball-milled LiAlH<sub>4</sub> doped with various metal chlorides (1:1 weight ratio, 3-6:1 molar ratio) together with the data of Al<sub>3</sub>Zr [16], Al<sub>3</sub>V [13], Al<sub>3</sub>Ni [13]. The diffraction peaks of the ball-milled LiAlH<sub>4</sub> doped with ZrCl<sub>4</sub> observed at 2θ of 38.2°, 44.5°, 64.7° and 77.7° correspond to those of cubic Al<sub>3</sub>Zr [16]. This means that Al<sub>3</sub>Zr with cubic structure is formed by a mechanochemical reaction of LiAlH<sub>4</sub> and ZrCl<sub>4</sub>.

Bragg peaks corresponding to LiCl and Al<sub>3</sub>V or Al<sub>3</sub>Ni are found in those XRD patterns.

Then LiAlH<sub>4</sub> and the transition metal chlorides take the following reaction path.



Mechanochemical reaction is an effective process for introducing metastable structure such as cubic Al<sub>3</sub>Ti [15] and cubic Al<sub>3</sub>Zr [16]. The transition metal trialuminides Al<sub>3</sub>X (Ti, Zr, V, Ni) intermetallic phases prepared by the mechanochemical reaction of metal chlorides and LiAlH<sub>4</sub> may act as dehydrogenation catalysts. Figure 4 also presents the XRD patterns of the ball-milled LiAlH<sub>4</sub> doped with ZnCl<sub>2</sub> together with the data of Zn, LiCl and Al. The diffraction peaks at 2θ of 43.3°, 34.9° and 38.6° are raised from (101), (200) and (111) planes of Zn, LiCl and Al, respectively. The reaction of LiAlH<sub>4</sub> and ZnCl<sub>2</sub> is represented as follows.



In the first transition series, the 3d-orbitals of Zn are fully occupied by electron. The occupied d-orbitals lose the catalytic activity [17]. Thus, vacant d-orbital correlates with the interaction between H<sub>2</sub> molecule and transition metals.

For the transition metals having d-hole, the percentage d-character of the metallic bond and the electronegativity are indicators of the electronic structure of the metal. The percentage d-character and the electronegativity have been correlated in an empirical way with catalytic data [17, 18]. Figure 5 displays the correlation of the H<sub>2</sub> desorption capacity during ball-milling with the percentage d-character and the electronegativity of the transition metals [17-19]. The capacity decreases with the percentage d-character. The behavior indicates that d-electron facilitates the interaction between transition metal and hydrogen by decreasing the percentage d-character. A smaller electronegativity gives a larger H<sub>2</sub> desorption capacity as shown in Figure 5. This means that the binding is ionic. The ionic binding between metal and hydrogen plays an important role for the catalytic activity. For transition metals, the heat of adsorption of hydrogen increases with decreasing of the percentage d-character. Therefore, the high catalytic activity of Ti and Zr might be achieved by strong chemisorption of hydrogen.

The ball-milled LiAlH<sub>4</sub> doped with 5 wt% of nano-Ni for 24 h desorbed 2.5 wt% of H<sub>2</sub> by the TPD measurement T<600 K. This indicated 5 wt% of H<sub>2</sub> was desorbed during ball-milling at room temperature, while the H<sub>2</sub> desorption capacities of the ball-milled LiAlH<sub>4</sub> doped with Ni was only 0.7 wt% at room temperature. It is clear from the results that H<sub>2</sub> desorption is remarkably improved by using the nano catalyst at room temperature. The structure of the ball-milled specimens doped with Ni and nano-Ni was characterized by the X-ray diffraction method. The XRD patterns of the ball-milled specimens are shown in Figure 6. We notice that the diffraction peak of the specimen at 51.8° is raised from (200) planes of Ni, in which the unit cell of Ni is cubic in shape. Thus it is suggested that the catalytic activity is improved with decreasing Ni particle size.

In the first step reaction (1), LiAlH<sub>4</sub> dissociates with the evolution of hydrogen to form Li<sub>3</sub>AlH<sub>6</sub> and Al. Then, the weight ratio of Al to Li<sub>3</sub>AlH<sub>6</sub> should be constant below H<sub>2</sub>

desorption capacity 5.3 wt%. The diffraction peaks of the specimen in Figure 6 at  $2\theta$  of  $21.9^\circ$  and  $38.5^\circ$  are assigned to the reflection of 100 for  $\text{Li}_3\text{AlH}_6$  and 111 for Al, respectively. The relative peak intensity  $I_{[\text{Al}(111)]}/I_{[\text{Li}_3\text{AlH}_6(100)]}$  is assumingly proportional to the weight ratio of  $\text{Li}_3\text{AlH}_6$  and Al. Figure 7 shows the relationship between the  $\text{H}_2$  desorption capacity of the ball-milled  $\text{LiAlH}_4$  doped with a catalyst and the relative peak intensity. We found that the catalysts are classified to two groups. The relative peak intensity of the specimen doped with  $\text{VCl}_3$ ,  $\text{NiCl}_2$ , Ni or nano-Ni is 3-8 and approximately independent of the capacity. We confirmed that the mechanochemical reaction of  $\text{LiAlH}_4$  in the presence of the catalysts induces the transformation of  $\text{LiAlH}_4$  into  $\text{Li}_3\text{AlH}_6$ , Al and  $\text{H}_2$  and is expressed by reaction (1). As shown in Figure 7, one can see that the intensity of the ball-milled  $\text{LiAlH}_4$  doped with  $\text{TiCl}_3$  or  $\text{ZrCl}_4$  is remarkably increased with the desorption capacity. The relative intensity of the ball-milled  $\text{LiAlH}_4$  doped with  $\text{TiCl}_3$  exceeds ten times of the specimen doped with another group of catalysts around the desorption capacity of 4 wt%. This can be understood by considering that doping with  $\text{TiCl}_3$  or  $\text{ZrCl}_4$  results in a hydrogen release due to the first step and second step reactions catalyzed by the product of reaction (3) below the  $\text{H}_2$  desorption capacity of 5 wt%.

It should be noted that reversible  $\text{H}_2$  absorption/desorption of  $\text{LiAlH}_4$  is one of the most important properties of the material, determining its potential for practical  $\text{H}_2$  storage applications. Although, it is obvious that  $\text{LiAlH}_4$  is not reversible because of its high dissociation pressure based on the low heat of formation [14]. Further studies are necessary to improve the reversibility. Partial atom substitutions and the mixture composed of other complex hydride may provide reversible hydrogen storage materials.

## Conclusions

We found that the  $H_2$  desorption capacity, which is an indicator of the catalytic activity, increased with decreasing of the percentage d-character, the electronegativity and the catalytic size of the transition metal. Doping with  $TiCl_3$  and  $ZrCl_4$  eliminated first and second steps of reactions (1), (2), while doping with other catalysts only eliminated first step reaction. It is presumed that the strong chemisorption ability of Ti and Zr towards hydrogen, which concludes in the formation of a metal-hydride phase, is responsible for the catalytic activity.

### **Acknowledgements**

The authors are greatly indebted to N. Suzuki of the Toyota Central R&D Labs., Inc. for his help and discussion.

### **FIGURE CAPTIONS**

Figure 1. XRD patterns of ball-milled  $LiAlH_4$  doped with  $TiCl_3$  and  $LiAlH_4$ , together with the data of  $Li_3AlH_6$ ,  $LiCl$ ,  $LiH$  and  $Al$ .

Figure 2. HRTEM image and EDS spectra of ball-milled  $LiAlH_4$  doped with  $TiCl_3$  for 24 h.

Figure 3. XRD patterns of ball-milled  $LiAlH_4$  doped with  $TiCl_3$ , together with the data of  $Al_3Ti$  and  $LiCl$ .

Figure 4. XRD patterns of ball-milled  $LiAlH_4$  doped with metal chloride (50 wt%), together with the data of  $Al_3V$ ,  $Al_3Ni$ ,  $Al_3Zr$ ,  $Zn$ ,  $LiCl$  and  $Al$ .

Figure 5. Correlation of  $H_2$  desorption capacity at room temperature with percentage d-character and electronegativity.

Figure 6. XRD patterns of ball-milled  $LiAlH_4$  doped with Ni and nano-Ni.

Figure 7. Relative peak intensity  $I_{[Al(111)]}/I_{[Li_3AlH_6(100)]}$  vs.  $H_2$  desorption capacity.

### **References**

- [1] Y. Kojima, Y. Kawai, S. Towata, T. Matsunaga, T. Shinozawa, M. Kimbara in Symposium GG, Materials and Technology for Hydrogen Storage and Generation, G-A., Nazri, C. Ping, R. C. Young, M. Nazri, J. Wang Eds., Mat. Res. Soc. Symp. Proc. **884E** (2005) GG6.5., Y. Kojima, Y. Kawai, S. Towata, T. Matsunaga, T. Shinozawa, M. Kimbara, J. Alloys Compd. (2006) in press.
- [2] D. Mori, N. Kobayashi, T. Shinozawa, T. Matsunaga, H. Kubo, K. Toh, M. Tsuzuki, J. Japan Inst. Metals **69** (2005) 308.
- [3] D. Mori, N. Kobayashi, T. Matsunaga, K. Toh, Y. Kojima, Mater. Japan **44** (2005) 257.
- [4] B. Bogdanović, M. Schwickardi, J. Alloys Compd. **253-254** (1997) 1.
- [5] B. Bogdanović, R. A. Brand, A. Marjanović, M. Schwickardi, J. Tölle, J. Alloys Compd. **302** (2000) 36.
- [6] C. M. Jensen, R. Zidan, N. Mariels, A. Hee, C. Hagen, Int. J. Hydrogen Energy **24** (1999) 461.
- [7] G. Sandrock, K. Gross, G. Thomas, C. Jensen, D. Meeker, S. Takara, J. Alloys Compd. **330-332** (2002) 696.
- [8] M. Fichtner, J. Engel, O. Fuhr, O. Kircher, O. Rubner, Mater. Sci. Eng. B, **108**, (2004) 42.
- [9] V. P. Balema, K. W. Dennis, V. K. Pecharsky, Chem. Commun. (2000) 1665.
- [10] V. P. Balema, V. K. Pecharsky, K. W. Dennis, J. Alloys Compd. **313** (2000) 69.
- [11] V. P. Balema, J. W. Wiench, K. W. Dennis, M. Pruski, V. K. Pecharsky, J. Alloys Compd. **329** (2001) 108.
- [12] M. Resan, M. D. Hampton, J. K. Lomness, D. K. Slattery, Int. J. Hydrogen Energy, **30** (2005) 1413.

- [13] "Powder Diffraction File," Publication Manager T. M. Kahmer, Editor-in-Chief W. F. McClune, Editor of Calculated Patterns S. N. Kabekkodu, Staff Scientist H. E. Clark, Database Programmer V. Bosnic, International Center for Diffraction Data (JCPDS), Pennsylvania USA (2004).
- [14] T. N. Dymova, D. P. Aleksandrov, V. N. Konoplev, T. A. Silina, A. S. Sizareva, *Russ. J. Coord. Chem.* **20** (1994) 263.
- [15] X. D. Kang, P. Wang, X. P. Song, X. D. Yao, G. O. Lu, H. M. Cheng, *J. Alloys Compd.* (2006) in press.
- [16] K. I. Moon, K. Y. Chang, K. S. Lee, *J. Alloys Compd.* **312** (2000) 273.
- [17] G. C. Bond, *Catalysis by Metal*, Academic Press, New York (1962).
- [18] J. R. Anderson, *Structure of Metallic Catalysts*, Academic Press, New York (1975).
- [19] L. Pauling, *The Chemical Bond*, Cornell University Press (1967).

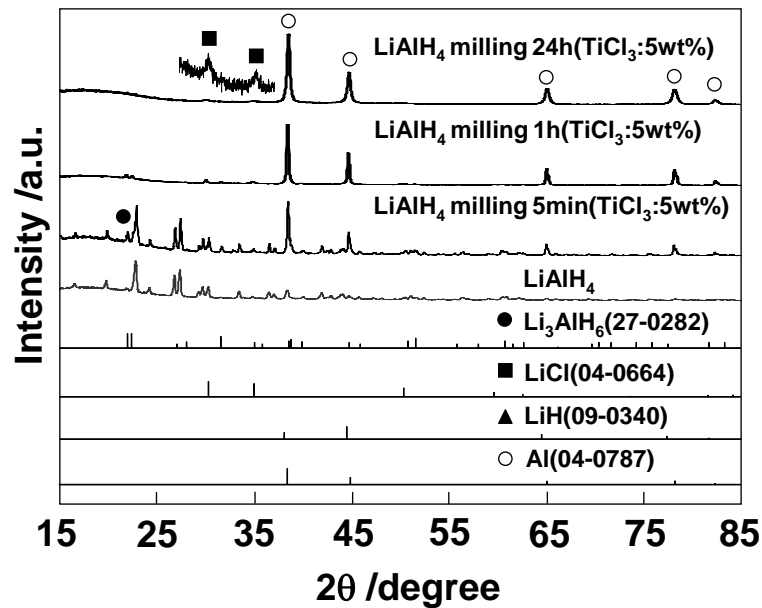


Figure 1. XRD patterns of ball-milled  $\text{LiAlH}_4$  doped with  $\text{TiCl}_3$  and  $\text{LiAlH}_4$ , together with the data of  $\text{Li}_3\text{AlH}_6$ ,  $\text{LiCl}$ ,  $\text{LiH}$  and  $\text{Al}$ .

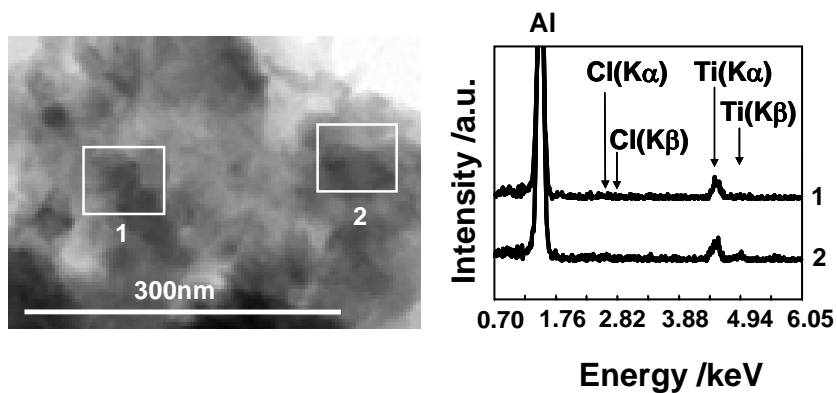


Figure 2. HRTEM image and EDS spectra of ball-milled  $\text{LiAlH}_4$  doped with  $\text{TiCl}_3$  for 24 h.

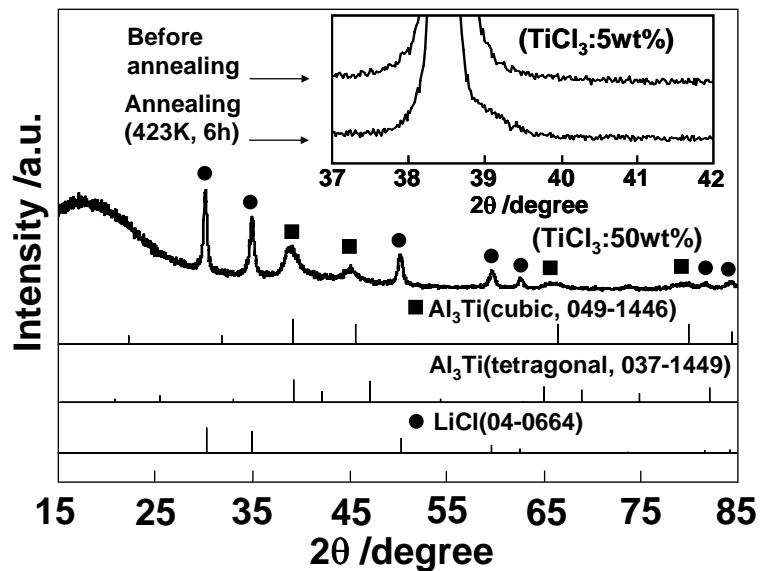


Figure 3. XRD patterns of ball-milled  $\text{LiAlH}_4$  doped with  $\text{TiCl}_3$ , together with the data of  $\text{Al}_3\text{Ti}$  and  $\text{LiCl}$ .

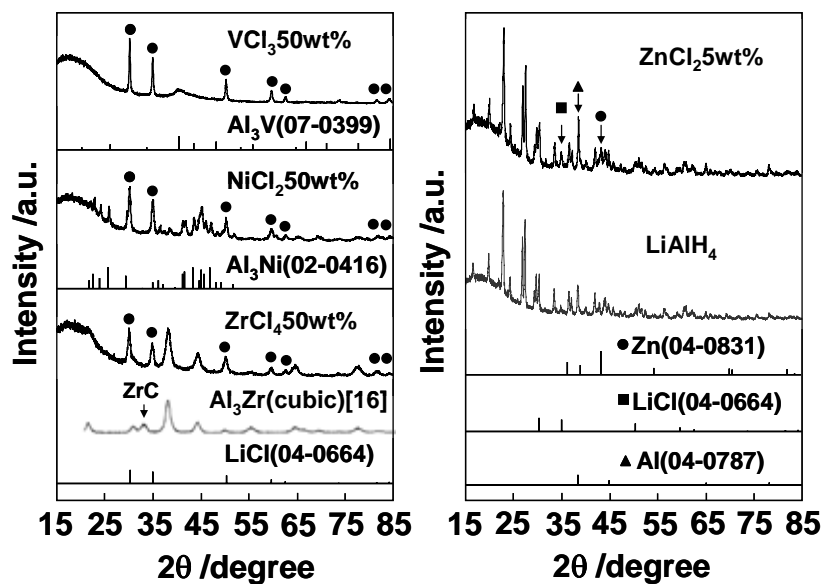


Figure 4. XRD patterns of ball-milled  $\text{LiAlH}_4$  doped with metal chloride (50 wt%), together with the data of  $\text{Al}_3\text{V}$ ,  $\text{Al}_3\text{Ni}$ ,  $\text{Al}_3\text{Zr}$ ,  $\text{Zn}$ ,  $\text{LiCl}$  and  $\text{Al}$ .

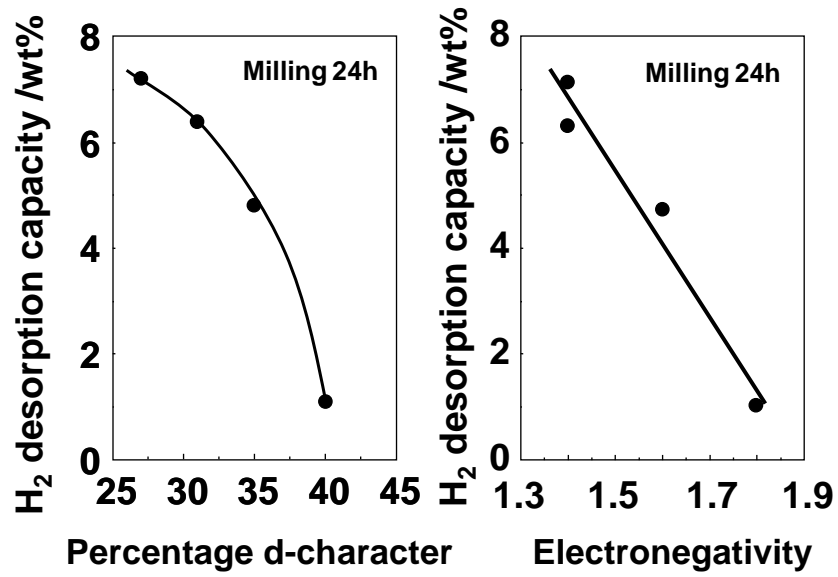


Figure 5. Correlation of H<sub>2</sub> desorption capacity at room temperature with percentage d-character and electronegativity.

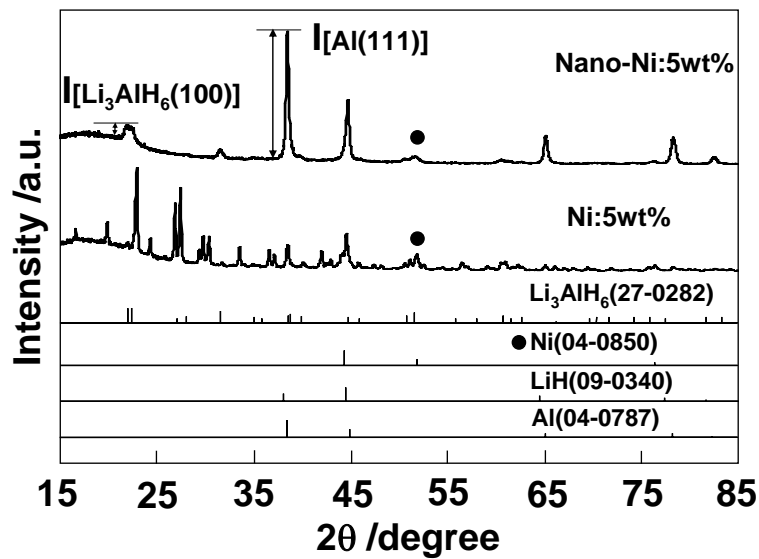


Figure 6. XRD patterns of ball-milled LiAlH<sub>4</sub> doped with Ni and nano-Ni.

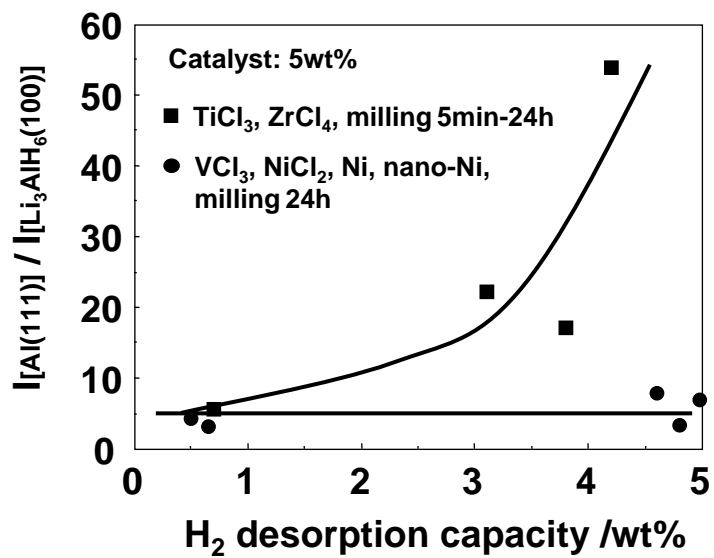


Figure 7. Relative peak intensity  $I_{\text{Al}(111)} / I_{\text{Li}_3\text{AlH}_6(100)}$  vs.  $\text{H}_2$  desorption capacity.